Functional analyses of chitinolytic enzymes in the formation of calcite prisms inPinctada fucata

Hiroyuki Kintsu
the University of Tokyo
Alberto Pérez-Huerta
University of Alabama
Shigeru Ohtsuka
the Univeristy of Tokyo
Taiga Okumura
the University of Tokyo
Shinsuke Ifuku
Tottori Daigaku
Koji Nagata
the University of Tokyo
Toshihiro Kogure
the Univeristy of Tokyo
Michio Suzuki (amichiwo@mail.ecc.u-tokyo.ac.jp)
the University of Tokyo https://orcid.org/0000-0001-6150-8957

Research article

Keywords: biomineralization, calcite, chitin, chitinolytic enzymes, Pinctada fucata, prismatic layer

Posted Date: December 23rd, 2019

DOI: https://doi.org/10.21203/rs.2.19558/v1

Functional analyses of chitinolytic enzymes in the formation of calcite prisms in *Pinctada fucata*.

Hiroyuki Kintsu[12], Alberto Pérez-Huerta[3], Shigeru Ohtsuka[4], Taiga Okumura[5], Shinsuke Ifuku[6], Koji Nagata[1], Toshihiro Kogure[5], Michio Suzuki[1]*

[1]Department of Applied Biological Chemistry, Graduate School of Agricultural and Life Sciences, The University of Tokyo, Tokyo 113-8657, Japan.

[2]National institute for environmental studies, Ibaraki 305-8506, Japan

[3]Department of Geological Sciences, The University of Alabama, Tuscaloosa AL 35487, USA.

[4]Institute of Engineering Innovation, The University of Tokyo, Tokyo 113-8656, Japan

[5]Department of Earth and Planetary Science, Graduate School of Science, The University of Tokyo, Tokyo, Japan.

[6]Department of Chemistry and Biotechnology, Graduate School of Engineering, The University of Tottori, Tottori, 680-8552, Japan.

* Corresponding author

e-mail: amichiwo@mail.ecc.u-tokyo.ac.jp

Abstract

Background: The mollusk shells present distinctive microstructures that are formed by small amounts of organic matrices controlling the crystal growth of calcium carbonate. These microstructures show superior mechanical properties such as strength or flexibility. The shell of *Pinctada fucata* has the prismatic layer consisting of prisms of single calcite crystals. These crystals contain small-angle grain boundaries caused by a dense intracrystalline organic matrix network to improve mechanical strength. Previously, we identified chitin and chitinolytic enzymes as components of this intracrystalline organic matrix. In this study, we analyzed the function of those organic matrices in calcium carbonate crystallization by *in vitro* and *in vivo* experiments.

Results: We analyzed calcites synthesized in chitin gel with or without chitinolytic enzymes by using transmission electron microscope (TEM) and atom probe tomography (APT). TEM observations showed that grain boundary was more induced as concentration of chitinolytic enzymes increased and thus, chitin became thinner. In an optimal concentration of chitinolytic enzymes, small-angle grain boundaries were observed. APT analysis showed that ion clusters derived from chitin were detected. In order to clarify the importance of chitinolytic enzymes on the formation of the prismatic layer *in vivo*, we performed the experiment in which chitinase inhibitor was injected into a living *Pinctada fucata* and then analyzed the change of mechanical properties of the prismatic layer. The hardness and elastic modulus increased after injection of chitinase inhibitor. Electron back scattered diffraction (EBSD) mapping data showed that the spread of crystal orientations in whole single crystal also increased by the effect of inhibitor injections.

Conclusion: Our results suggested that chitinolytic enzymes may function cooperatively with chitin to regulate the crystal growth and mechanical properties of the prismatic layer, and chitinolytic enzymes are essential for the formation of the normal prismatic layer of *P. fucata*.

Keywords: biomineralization, calcite, chitin, chitinolytic enzymes, *Pinctada fucata*, prismatic layer

Background

Molluscan shells consist of more than 90% calcium carbonate and small amounts of organic matrices, which interact with calcium carbonate and regulate its crystallization. The organic matrices may be classified into three groups: insoluble organic matrices (IOMs) such as chitin [1–4], soluble organic matrices (SOMs) binding IOMs with a

domain that can interact with IOMs [5–8], and SOMs that exist freely [9–11]. IOMs generally provide the scaffold for crystallization, and SOMs contain acidic domains such as Asp-rich regions, which control the crystal polymorph, morphology, and growth. Such organic-inorganic interactions can generate a fine microstructure. However, most of the detailed structures and functions of these organic molecules are still unknown.

Pinctada fucata, a bivalve used for pearl cultivation, has a microstructure composed of a prismatic layer in its shell. The prismatic layer exists on the outer layer of shells, and is comprised of calcite prisms surrounded by an organic framework, which appears as a honeycomb structure [12, 13]. The radius and length of one calcite prism are approximately 50 μm and 150 μm, respectively (Fig. 1a, b). Previous studies have reported that the calcite prism of *P. fucata* exhibits unique characteristics. Transmission electron microscopy (TEM) has revealed that the calcite prism of *P. fucata* is not a complete single crystal, but contains small angle grain boundaries, which are slight crystal misorientations [14, 15]. TEM has also shown that organic matrices are localized in a network, and that the locations of the organic networks correspond to small angle grain boundaries, indicating that the organic networks might contribute to the formation of small angle grain boundaries [16], which may improve the strength and toughness of the prismatic layer. A calcite prism of *P. fucata* is harder than a calcite prism of other species such as *Atrina pectinata*, which does not contain small angle grain boundaries as in abiogenic calcite crystals. Small angle grain boundaries could prevent the penetration of cracks when a force is applied to the crystals [17]. Basically, calcite easily fractures along a {104} cleavage plane because of the high density of atoms in this cleavage plane. Although the high density of atoms within one plane stabilizes it by retaining the atoms within one plane, it also reduces the attachment energy which holds parallel planes

together [18]. Thus, small angle grain boundaries, which are distortions of atomic arrangements, may change energy balances and prevent penetration of cleavage, leading to improvement of mechanical properties of calcite prisms. Surprisingly, although it is difficult to artificially mimic the superior microstructure of calcite prisms, *P. fucata* easily produces these fine structures under normal temperature and pressure using organic matrices.

Recently, we characterized the mechanism of formation of small angle grain boundaries by focusing on the components of the organic networks. From organic networks, chitin was identified as the primary component [19]. In addition, the chitinolytic enzymes that degrade chitin were also identified when the proteins that formed a complex with chitin were analyzed. *In vitro* experiments revealed that when calcium carbonate was crystallized in chitin gel treated with chitinolytic enzymes, the lattice distortion of the synthesized crystal increased, depending on the concentration of enzymes. This finding indicated that chitin and chitinolytic enzymes might work cooperatively to induce small angle grain boundaries. In this study, we analyzed the synthesized calcium carbonate crystals in detail to reveal how the chitin condition was changed by degradation with chitinolytic enzymes. Furthermore, to demonstrate the importance of chitinolytic enzymes in the formation of the prismatic layer, we injected an inhibitor of chitinolytic enzymes into living *P. fucata* and examined whether the mechanical properties of calcite prisms were changing by inhibiting the activity of chitinolytic enzymes. These results provide new insights into the field of biomineralization.

Results and Discussion

Identification of components in an intracrystalline organic network

Previous reports have shown that small angle grain boundaries correspond to the position of an intracrystalline organic network, suggesting that the intracrystalline organic network was related to the formation of small angle grain boundaries [16]. It was therefore important to characterize the structure of components in an intracrystalline organic network. The extraction scheme is described in Figure 1c. To extract organic matrices from the intracrystalline organic network, the calcite prism was decalcified with acetic acid and the resulting organic matrices were classified as acid-insoluble or acid-soluble. The organic network was mainly comprised of acid-insoluble organic matrices. Generally, the acid-insoluble organic matrices from the molluscan shell are comprised of complexes of proteins and sugars such as chitin. The protein components can be extracted by detergents such as sodium dodecyl sulfate (SDS). Detergent-soluble organic matrices (DSOMs) were resolved by SDS-PAGE and detergent-insoluble organic matrices (DIOMs) were analyzed by Fourier-transform infrared spectroscopy, which revealed that DIOMs were composed of chitin, with polysaccharides comprised of *N*-acetyl-D-glucosamine (NAG) (Fig. 1d) [19]. Two types of chitin polymorphs have been reported. The chains of β-chitin bind each other in an antiparallel arrangement [20]. However, β-chitin is involved in the parallel chain containing water between chains [21]. Chitin identified from molluscan species to date is β-chitin. When the band patterns of acid-soluble organic matrices were compared to that of DSOMs, a specific band with high molecular weight components was detected in DSOMs (Fig. 1e). The band was removed and digested with trypsin to determine the amino acid sequence by liquid chromatography–mass spectrometry/mass spectrometry. The identified protein in this band was a complex of chitinolytic enzymes (gene ID: pfu_aug1.0_10761.1_31980 and

pfu_aug1.0_6745.1_67528). The chitinolytic enzymes can degrade the chitin chain. A BLAST search identified these proteins as chitinase and β-*N*-acetylhexosaminidase; the enzymes were named PfCN and PfCB, respectively. PfCN is composed of 466 amino acids with a molecular mass of 53.9 kDa, and belongs to the glycoside hydrolase (GH) family 18. The sequence of PfCN includes a signal peptide in the N-terminus and GH18 domain (Fig. 1f). PfCB is composed of 662 amino acids with a molecular mass of 72 kDa and belongs to the GH20 family. The sequence of PfCB includes the GH20 domain (Fig. 1f). Chitinolytic enzymes can be classified into two groups: exo or endo. β-*N*-acetylhexosaminidases, which belong to the GH20 family, are exoenzymes that degrade chitin from the nonreducing end to produce NAG. Chitinases of animals mainly belong to the GH18 family (some chitinases from plants and bacteria belong to the GH19 family) and degrade chitin randomly to produce $(NAG)_2$ [22, 23].

To investigate the true activity of chitinolytic enzymes, DSOMs were applied to native PAGE containing glycol chitin in the gel. These previous results suggested that the complex of chitinolytic enzymes kept enzymatic activity in the shell [19]. Although chitin has been identified in various kinds of molluscan shells, which provide scaffolds for crystallization [1, 4, 24], only a few chitinolytic enzymes have been identified from molluscan shells, and their functions in shells are unknown [25–27]. Because chitinolytic enzymes binding chitin were identified from calcite prisms and possessed the ability to degrade chitin in the shell, we identified the cooperative functions of chitin and chitinolytic enzymes involved in the formation of small angle grain boundaries in calcite prisms.

Synthesis of calcium carbonate crystals in chitin gel treated with chitinolytic

enzymes *in vitro*

During formation of the prismatic layer, the organic frameworks are constructed before calcification. The space surrounded by the organic frameworks is filled with organic gel solution comprised mainly of chitin and matrix proteins, then calcium carbonate is crystallized with organic gel solution in the space [13, 28]. We identified the chitinolytic enzymes as matrix proteins in the organic network. The organic gel solution containing chitin and chitinolytic enzymes can develop into organic networks during formation of the prismatic layer and affect calcite crystallization. To investigate how chitin and chitinolytic enzymes affect the formation of calcite crystals, we performed an *in vitro* calcium carbonate crystallization experiment using chitin gel and chitinolytic enzymes (Fig. 2a).

The chitin gel was prepared by dissolving chitin powder in methanol saturated with calcium chloride dehydrate. The chitin solution was then added to a large amount of water for gelatinization. Calcium carbonate was crystallized in the chitin gel with or without yatalase, a commercially available chitinolytic enzyme containing the activities of both GH18 and GH20 produced by a strain of *Streptomyces*. Because we identified both GH18 and GH20 family chitinolytic enzymes in the prismatic layer, yatalase was an appropriate mimicking agent of the chitinolytic enzymes in this layer. The treated chitin gel was washed with calcium chloride solution and incubated in the desiccator with ammonium carbonate powder to supply CO_2 gas, which dissolved in the chitin gel and became a carbonate ion. Electrostatic coupling of the carbonate ion and calcium ion in the chitin gel induced crystallization of calcium carbonate. Following crystallization, calcium carbonate crystals were collected by dissolving only the chitin gel with sodium hypochlorite; the remaining crystals were observed using scanning electron microscopy

(SEM). The normal shape of calcium carbonate crystals (a typical rhombohedral calcite) was formed in the chitin gel without yatalase treatment (Fig. 2b). Conversely, the shape of calcite crystals became polygonal in the chitin gel treated with 0.12 mg/mL chitinolytic enzymes (Fig. 2c). In the chitin gel treated with 1.2 mg/mL chitinolytic enzymes, the shape of the calcite crystal was completely changed and appeared to be round (Fig. 2d). Chitin likely aggregated between polysaccharide chains via hydrogen bonding. Chitinolytic enzymes degraded the surface of the aggregated fiber of chitin and decreased fiber thickness. The results of Fig. 2b–d suggested that as the concentration of chitinolytic enzymes increased, the chitin fiber became thinner, and the surface microstructure of the calcite crystals in the chitin gel changed. To confirm that thin chitin fibers had effects on crystallization, we used chitin nanofibers instead of chitin gel in the crystallization experiment. Chitin nanofibers were made by mechanically grinding chitin powder from crab shells under acidic conditions to facilitate fibrillation and obtain a uniform thickness with a width of 10–20 nm [29]. When calcium carbonate crystals synthesized in the chitin nanofiber solution were observed using SEM, the shape of the calcite crystals was polygonal, similar to crystals in the presence of 0.12 mg/mL enzymes (Fig. 2e). This change in crystal morphology was likely because of the potential change of chitin fibers attaching to the growth surface of crystals. The thick chitin fiber (0 mg/mL) may not have as much potential because it could not attach to the growth surface, resulting in a few steps involving substances absorbed on the growth surface. However, as the chitin fibers became thinner, the number of crystal steps increased. In addition, each step was not aligned, and slightly rotated. Thus, the crystals gradually formed a round shape because the chitin fibers become thinner.

These results suggested that chitin directly interacted with and affected the

morphology of calcium carbonate. Chitin is a polymer composed of NAG, which possesses an acetyl amino group at C6, whereas cellulose is composed of glucose molecules with hydroxyl groups. To investigate the specific function of chitin in calcium carbonate crystallization, we used a cellulose gel to compare the results. When calcium carbonate was crystallized in a cellulose gel with or without treatment of cellulase at concentrations of 0, 0.12, and 1.2 mg/mL, rhombohedral crystals were observed at all concentrations, indicating that cellulose had no effect on crystallization (Fig. S1). Because an acetyl amino group has both negative and positive charges, the acetyl amino group may interact with calcium and carbonate ions in calcium carbonate crystals during crystal growth.

Analysis of synthesized calcium carbonate crystals

TEM bright field images of the cross-sections prepared by a focused ion beam revealed that the calcite crystal formed in the chitin gel without yatalase treatment contained many thick chitin fibers with a bright contrast, and typical interference fringes of equal inclination of single crystals were observed (Fig. 3a), indicating that chitin gel without chitinolytic enzyme treatment did not affect calcium carbonate. In addition, electron diffraction patterns of selected areas indicated that the calcium carbonate crystals synthesized in these conditions were single crystals (Fig. S2). By contrast, following 0.12 mg/mL chitinolytic enzyme treatment (Fig. 3b), slightly disordered lines of fringes were partially observed. If the sample was a perfect single crystal, equal inclination interference fringes would have shown clear lines. At a concentration of 0.12 mg/mL, fringe lines were interrupted by lattice distortions such as small angle grain boundaries. Furthermore, the positions of partial interrupted fringes corresponded to that of chitin

fibers. Thus, chitin might induce the small angle grain boundaries in calcium carbonate crystals. At 1.2 mg/mL (Fig. 3c), thin chitin fibers were embedded with calcium carbonate. The selected area electron diffraction pattern of the crystal was vastly different between the boundaries of chitin fibers. Combined with the electron diffraction patterns, the calcite crystal was polycrystal. In the chitin nanofiber solution, the fringes were disordered throughout the entire area (Fig. 3d). Based on these results, TEM observation also supported the possibility that lattice distortion increased as the chitin fibers were degraded by chitinolytic enzymes, because the increasing surface areas of the chitin fibers strengthened the physical and/or chemical interactions between calcium carbonate and the chitin fiber. This strong interaction may have allowed chitin fibers to attach to the crystal growth front and inhibit growth of the crystal face in a random manner to induce a rounded shape.

To examine the interaction of chitin with calcium carbonate crystals in detail, these crystals were analyzed by atom probe tomography (APT). APT is a useful technique to determine the three-dimensional (3D) distribution of atoms or ions in different materials [30–32]. In APT analysis, the specimen shaped into a needle-like tip with a radius of 50–100 nm by a focused ion beam was ionized by field evaporation to detect atoms of ions with 2D ion distributions, followed by a 3D reconstruction. In Fig. 3e-h, the 3D reconstruction images show that ion clusters of COH^+ (yellow) and COH_2^+ (pink) derived from chitin are detected within calcium carbonate ions (red). Fragments of chitin were partially detected in calcium carbonate at a concentration of 0 mg (Fig. 3e). Most of signals were localized in the edge of sample. When the thick chitin fibers were embedded in the tip, the tip was broken, because thick chitin fiber is soft and decreased the strength of the tip. The localized signal of the edge may be derived from the neighbor chitin thick

fiber outside the tip. On the other hand, chitin signals increased and were distributed in wide area within calcium carbonate at higher concentrations (Fig. 3f, g). Since both homogeneous and continuous signals were observed in all area, these signals were likely to be both chitin oligomers and chitin nanofibers degraded by chitinolytic enzymes. These APT results support the hypothesis that chitin without the treatment of enzyme has no effect on the crystal formation and the effect of the chitinolytic enzymes on the crystallization becomes higher as the concentration increases. In case of the artificial chitin nanofiber produced by chemical and physical procedure, high density signals derived from chitin were detected (Fig. 3h). This probably indicates that the artificial chitin nanofiber has high dispersibility and can be involved in the tip, because the nanofiber does not affect the strength of the tip.

The influence of chitinase inhibitor injection on the formation of calcite prisms of *P. fucata in vivo*

As previously mentioned, we showed that chitinolytic enzymes may play important roles in formation of the *P. fucata* prismatic layer. To show the importance of chitinolytic enzymes on the formation of the prismatic layer, allosamidin, an inhibitor of GH18 chitinase [33], was injected into a living *P. fucata* every 3 days for a month. Chitinases hydrolyze β-1,4 linkages of the chitin polymer randomly to produce chitin oligomers, especially chitobiose, followed by β-*N*-acetylhexosaminidases, which degrade chitin oligomers into NAG because β-*N*-acetylhexosaminidases prefer short oligosaccharides [34, 35]. It is therefore important to use allosamidin to evaluate the effect of chitinolytic enzymes. Following injection, *P. fucata* was grown in natural sea water. Measurement of chitinase activity from mantle extracts showed that allosamidin suppressed activity for 1

month, indicating that the shell was formed under conditions of low chitinase activity (Fig. S3). If our hypothesis that chitinolytic enzymes degrade chitin and affect crystal growth was correct, the prism should be affected by inhibition of activity. Fig. 4a and b shows microdiffraction mapping of the longitudinal cross-section of prismatic layers along the *c* axis and line profiles of one prism. In the normal prismatic layer without inhibitor, the color of one prism was found to be uniform from mapping the image and angle spread of one prism measured from the line profile within 3 degrees; there was minimal crystal disorientation within one prism. However, in the prismatic layer treated with inhibitor, the crystal orientation of one prism was found to be gradually changed, with the mapping image and angle spread of one prism approximately 10 degrees. The reason for the increase of angle spread was likely due to intracrystalline chitin thickening from inhibiting chitin degradation. We previously reported that thicker chitin fibers inside the calcite prism treated with allosamidin compared with those of normal calcite prism were observed using TEM. Chitin fibers that increased in thickness may have contributed to crystal disorientation.

A previous study reported that a biotic calcite crystal with slight crystal distortion was stronger than an abiotic calcite crystal without crystal distortion [36] because the abiotic calcite is easily cracked under high pressure. The crystal distortion blocked transmission of strength to inhibit propagation. Because allosamidin treatment caused crystal distortions in calcite prisms, we investigated how such crystal distortions influenced mechanical properties such as hardness and the elastic modulus of calcite prisms. To examine the mechanical properties of calcite prisms, nanoindentation analysis of the prism surface was conducted. A nanoindentation force-displacement curve was drawn from the applied load versus depth profile, and hardness and the elastic modulus

were obtained from this curve. The force-displacement curves are shown in Fig. 4c and d. When a force was loaded up to 100 mN, the maximum displacement was approximately 1–3 μm in the non-injection treatment (measurements at eight points). However, with allosamidin treatment, the maximum displacement was approximately 1–1.5 μm (measurements at six points). In addition, the cracks caused by indentation following allosamidin treatment were blocked to a greater extent than the non-injection treatment (Fig. S4), and both hardness and the reduced elastic modulus of prisms following allosamidin treatment increased by approximately 80.6% and 105%, respectively, compared with those of the non-injection treatment (Fig. 4e). These results indicated that inhibition of chitinase activity strengthened prisms, likely because crystal defects observed by electron backscatter diffraction (EBSD) could prevent the motion of dislocation in a crystal. Crystals contain a few dislocations that exist along the end of an extra half-plane of atoms [37]. Because the force field around dislocation creates a strain, a dislocation easily moves along the plane perpendicular to the end of an extra half-plane when a shear stress is applied. The dislocation motion causes a slip of the crystal plane. Thus, reducing the dislocation motion results in enhanced mechanical strength. A grain boundary caused by a disorientation or enclosing substance is one factor that can reduce the dislocation motion. This theory could enable us to examine why a biotic calcite containing slight crystal distortions was stronger than abiotic calcite. In the present study, because micro-EBSD mapping revealed crystal disorientation in prisms treated with an inhibitor, this crystal defect may have resulted in harder prisms than normal.

Conclusion

This study showed a novel mechanism of calcite prisms during shell formation. We

identified chitin and chitinolytic enzymes as the components of intraorganic matrices included in the calcification of prisms in the prismatic layer. Also, we show that both organic matrices worked cooperatively to provide superior mechanical properties to a prism calcite. Previous studies have reported that chitinolytic enzymes are expressed in some species of bivalves, but showed no clear evidence that chitinolytic enzymes were associated with calcification. Because it is known that chitinolytic enzymes in animals or plants are used to resist a bacterial infection, chitinolytic enzymes in bivalves are also considered to be involved in the immune system. Our study could therefore provide new possibilities for further development of biomineralization and material engineering.

Material and method

Purification and analysis of organic matrices from calcite prisms

The Japanese pearl oyster *P. fucata* was cultured at Ago Bay by Fisheries Research Division, Mie Prefecture Science and Technology Promotion Center in Japan. The prismatic layer was cut off from the dried 20 shells of *P. fucata*. The prismatic layer was treated with 50% sodium hypochlorite (nacalai, Japan) to remove the organic framework surrounding each calcite prism. After calcite prisms were decalcified with 1 M acetic acid at 4°C, AIOM and ASOM was collected. The acid-soluble fraction was concentrated by ultrafiltration tube (M.W. 10,000 cut off). To extract binding proteins from AIOM, AIOM was boiled with 1% SDS/10 mM DTT/50 mM Tris-HCl (pH 8.0) (detergent solution) for 10 min and DIOM and DSOM were obtained. ASOM and DSOM were applied to SDS-PAGE (15% acrylamide gel), followed by staining with Coomassie Brilliant Blue R-250. To identify proteins, the band was digested with trypsin and LC-MS/MS analysis was performed in an Orbitrap VEROS ETD system (Thermo Fisher Scientific, Carlsbad, CA, USA) according to the previous method [38]. Proteins were identified by using the genome database of *P. fucata* (OIST marine genomics unit;

https://marinegenomics.oist.jp/).

Synthesis of calcium carbonate in the chitin hydrogel

Chitin hydrogel was prepared according to the previous method [39]. The prepared chitin hydrogel was treated with Yatalase (an enzyme complex containing chitinase and chitobiase activities from *Corynebacterium* sp. OZ-21; TaKaRa) as chitinolytic enzyme. Yatalase was added to this chitin hydrogel in various concentrations and stirred for 24 hours. After reaction, chitin hydrogel was filtered and washed with 10 mM calcium chloride to remove Yatalase. The washed chitin hydrogel was spread on a plate (33.5 mm x 33.5 mm). This plate was put into desiccator filled with the gas of 5 g of ammonium carbonate (Kanto Chemical), followed by the calcium carbonate crystallization in the chitin hydrogel for 24 h. Chitin hydrogel was dissolved with 50% sodium hypochlorite to collect the calcium carbonate crystals.

Calcium carbonate crystallization using chitin nanofiber

1.1% (w/v) chitin nanofiber in 0.5% acetic acid solution was prepared [29]. The chitin nanofiber solution was neutralization with 1 M NaOH. 10 mM calcium chlorite solution was added to the chitin nanofiber solution. Calcium carbonate was then crystallized in the chitin nanofiber solution using the same method described above. The formed calcium carbonate crystals were observed with SEM and the cross-sections prepared by FIB were observed by TEM.

TEM observations of the calcium carbonate crystals

The calcium carbonate crystals synthesized in the chitin hydrogel were washed with distilled water to remove the sodium hypochlorite. The inside of these calcium carbonate crystals was also observed by TEM to investigate the inside detailed microstructure. Electron-transparent thin specimens for TEM observation were prepared using a focused

ion beam (FIB) (FB 2100, Hitachi). The samples were locally coated with tungsten and trimmed using Ga ion beam and thinned down to a final thickness of 200 nm. These electron-transparent specimens were observed with a JEM-2010UHR TEM (JEOL) operated at 200 kV. The intracrystalline organic matrices were imaged by Fresnel contrast, not focusing on the organic matrices.

Atom probe tomography

The method of ATP analysis was performed according to previous study [32]. Briefly, the tip specimens of the synthesized calcium carbonate crystals were prepared with a radius of about 50 nm by using FIB. These specimens were ionized with the local electrode (LEAP 3000 XSi) of The University of Alabama. Parameters were following; laser pulse energy = 150 and 1300 pJ, detection rate = 2%, base temperature = 50 K. Three dimensional reconstructions from data of ion distributions were performed using the CAMECA IVAS software platform (details in [40]).

EBSD micrography of the prismatic layer

Before EBSD analysis, samples of the prismatic layer were embedded in epoxy (Buehler) and cut with ISOMET (Buehler) to expose the surface of the prismatic layer. The surface of specimen was polished with decreasing silicon carbide powder (32, 13 and 8 µm), subsequently with diamond suspension (6 µm), and finally with colloidal silica (0.06 µm). Crystallographic information including crystal phase and grain orientation on the surfaces was analyzed by a field emission scanning electron microscope (FE-SEM, JSM-7000F, JEOL Ltd.) equipped with electron back scattered diffraction.

Abbreviation

APT; atom probe tomography; BLAST: basic local alignment search; DIOMs: detergent-

insoluble organic matrices; DSOMs: detergent-soluble organic matrices; EBSD: electron back scattered diffraction; FIB: focused ion beam; FT-IR: fourier transform infrared spectroscopy; GH: glycoside hydrolase; LC-MS/MS: liquid chromatograph-tandem mass spectrometer; NAG: *N*-acetyl-D-glucosamine; IOMs: insoluble organic matrices; PAGE: polyacrylamide gel electrophoresis; SDS: sodium dodecyl sulfate; SEM: scanning electron microscope; SOMs: soluble organic matrices; TEM: transmission electron microscope;

Competing interests

The authors declare that they have no competing interests.

Availability of Data and Materials

All data in this study are included in this published article and its supplementary file.

Author's contribution

HK designed the study, performed the experiments, analyzed the data and drafted the manuscript. APH performed the APT analysis. SO performed EBSD measurement. OK and TK analyzed TEM observation. SI produced and provided chitin nanofibers. KN analyzed the data. MS designed the study and analyzed the data. All authors read and approved final manuscript

Funding

This research was partially funded by an Israel Science Foundation (ISF) – Japan Society for the Promotion of Science (JSPS) Joint Academic Research Program, Grant-in-Aid for Young Scientists B (JP16K20995), Grant-in-Aid for Scientific Research B (JP19H03045), Grant-in-Aid for Scientific Research on Innovative Areas IBmS: JSPS KAKENHI Grant Number JP19H05771 to MS, Grant-in-Aid for JSPS Fellows (DC2) to HK. A. P-H.

acknowledges support for the APT work from the U.S. National Science Foundation (NSF), grant number EAR-1647012.

Acknowledgements

We thank Takuya Akiyama in the university of Tokyo for sharing FT-IR instruments, and also thank Naoshi Kakio at Shimadzu corporation for helping the nanoindentation analysis.

References

1. Weiner S, Traub W. X-ray diffraction study of the insoluble organic matrix of mollusk shells. FEBS Lett. 1980;111:311–6
2. Weiner S, Traub W, Parker SB. Macromolecules in Mollusc Shells and Their Functions in Biomineralization. Philos Trans R Soc London B, Biol Sci. 1984;304:425–34
3. Levi-Kalisman Y, Falini G, Addadi L, Weiner S. Structure of the Nacreous Organic Matrix of a Bivalve Mollusk Shell Examined in the Hydrated State Using Cryo-TEM. J Struct Biol. 2001;135:8–17
4. Suzuki M, Sakuda S, Nagasawa H. Identification of chitin in the prismatic layer of the shell and a chitin synthase gene from the Japanese pearl oyster, *Pinctada fucata*. Biosci Biotechnol Biochem. 2007;71:1735–44
5. Suzuki M, Saruwatari K, Kogure T, Yamamoto Y, Nishimura T, Kato T, et al. An acidic matrix protein, Pif, is a key macromolecule for nacre formation. Science. 2009;325:1388–90
6. Montagnani C, Marie B, Marin F, Belliard C, Riquet F, Tayalé A, et al. Pmarg-Pearlin is a Matrix Protein Involved in Nacre Framework Formation in the Pearl Oyster *Pinctada margaritifera*. ChemBioChem. 2011;12:2033–43
7. Suzuki M, Iwashima A, Tsutsui N, Ohira T, Kogure T, Nagasawa H. Identification and Characterisation of a Calcium Carbonate-Binding Protein, Blue Mussel Shell Protein (BMSP), from the Nacreous Layer. ChemBioChem. 2011;12:2478–87
8. Marie B, Zanella-Cléon I, Corneillat M, Becchi M, Alcaraz G, Plasseraud L, et al. Nautilin-63, a novel acidic glycoprotein from the shell nacre of *Nautilus macromphalus*. FEBS J. 2011;278:2117–30
9. Miyamoto H, Miyashita T, Okushima M, Nakano S, Morita T, Matsushiro A. A carbonic anhydrase from the nacreous layer in oyster pearls. Proc Natl Acad Sci U S A. 1996;93:9657–60
10. Sudo S, Fujikawa T, Nagakura T, Ohkubo T, Sakaguchi K, Tanaka M, et al. Structures of mollusc shell framework proteins. Nature. 1997;387:563–4
11. Weiner S, Hood L. Soluble Protein of the Organic Matrix of Mollusk Shells: A Potential Template for Shell Formation. Science. 1975;190:987–9
12. Nakahara H, Bevelander G. The formation and growth of the prismatic layer of *Pinctada radiata*. Calcif Tissue Res. 1971;7:31–45
13. Checa AG, Rodríguez-Navarro AB, Esteban-Delgado FJ. The nature and formation of calcitic columnar prismatic shell layers in pteriomorphian bivalves. Biomaterials. 2005;26:6404–14

14. Okumura T, Suzuki M, Nagasawa H, Kogure T. Characteristics of biogenic calcite in the prismatic layer of a pearl oyster, *Pinctada fucata*. Micron. 2010;41:821–6
15. Gilbert PUPA, Young A, Coppersmith SN. Measurement of c-axis angular orientation in calcite (CaCO3) nanocrystals using X-ray absorption spectroscopy. Proc Natl Acad Sci U S A. 2011;108:11350–5
16. Okumura T, Suzuki M, Nagasawa H, Kogure T. Microstructural variation of biogenic calcite with intracrystalline organic macromolecules. Cryst Growth Des. 2012;12:224–30
17. Olson IC, Metzler RA, Tamura N, Kunz M, Killian CE, Gilbert PUPA. Crystal lattice tilting in prismatic calcite. J Struct Biol. 2013;183:180–90
18. Weiner S, Addadi L. Design strategies in mineralized biological materials. J Mater Chem. 1997;7:689–702
19. Kintsu H, Okumura T, Negishi L, Ifuku S, Kogure T, Sakuda S, et al. Crystal defects induced by chitin and chitinolytic enzymes in the prismatic layer of *Pinctada fucata*. Biochem Biophys Res Commun. 2017;489:89–95
20. Ogawa Y, Kimura S, Wada M, Kuga S. Crystal analysis and high-resolution imaging of microfibrillar α-chitin from Phaeocystis. J Struct Biol. 2010;171:111–6
21. Ogawa Y, Kimura S, Wada M. Electron diffraction and high-resolution imaging on highly-crystalline β-chitin microfibril. J Struct Biol. 2011;176:83–90
22. Henrissat B. A classification of glycosyl hydrolases based on amino acid sequence similarities. Biochem J. 1991;280:309–16
23. Henrissat B, Bairoch A. New families in the classification of glycosyl hydrolases based on amino acid sequence similarities. Biochem J. 1993;293:781–8
24. Weiss IM, Schönitzer V. The distribution of chitin in larval shells of the bivalve mollusk *Mytilus galloprovincialis*. J Struct Biol. 2006;153:264–77
25. Liu C, Li S, Kong J, Liu Y, Wang T, Xie L, et al. In-depth proteomic analysis of shell matrix proteins of *Pinctada fucata*. Sci Rep. 2015;5:1–14
26. Li H, Wang D, Deng Z, Huang G, Fan S, Zhou D, et al. Molecular characterization and expression analysis of chitinase from the pearl oyster Pinctada fucata. Comp Biochem Physiol Part B Biochem Mol Biol. 2017;203:141–8
27. Okada Y, Yamaura K, Suzuki T, Itoh N, Osada M, Takahashi KG. Molecular characterization and expression analysis of chitinase from the Pacific oyster *Crassostrea gigas*. Comp Biochem Physiol Part B Biochem Mol Biol. 2013;165:83–9
28. Checa AG. A new model for periostracum and shell formation in Unionidae (Bivalvia, Mollusca). Tissue Cell. 2000;32:405–16
29. Ifuku S, Nogi M, Yoshioka M, Morimoto M, Yano H, Saimoto H. Fibrillation of dried chitin into 10-20 nm nanofibers by a simple grinding method under acidic conditions. Carbohydr Polym. 2010;81:134–9
30. Valley JW, Cavosie AJ, Ushikubo T, Reinhard DA, Lawrence DF, Larson DJ, et al. Hadean age for a post-magma-ocean zircon confirmed by atom-probe tomography. Nat Geosci. 2014;7:219–23
31. Gordon LM, Tran L, Joester D. Atom Probe Tomography of Apatites and Bone-Type Mineralized Tissues. ACS Nano. 2012;6:10667–75
32. Pérez-Huerta A, Laiginhas F, Reinhard DA, Prosa TJ, Martens RL. Atom probe tomography (APT) of carbonate minerals. Micron. 2016;80:83–9
33. Sakuda S, Isogai A, Matsumoto S, Suzuki A. Search for microbial insect growth regulators. II. Allosamidin, a novel insect chitinase inhibitor. J Antibiot (Tokyo). 1987;40:296–300
34. Tews I, Perrakis A, Oppenheim A, Dauter Z, Wilson KS, Vorgias CE. Bacterial chitobiase structure provides insight into catalytic mechanism and the basis of

Tay–Sachs disease. Nat Struct Biol. 1996;3:638–48
35. Yang Q, Liu T, Liu F, Qu M, Qian X. A novel *β*-N-acetyl-d-hexosaminidase from the insect *Ostrinia furnacalis* (Guenée). FEBS J. 2008;275:5690–702
36. Kim Y-Y, Carloni JD, Demarchi B, Sparks D, Reid DG, Kunitake ME, et al. Tuning hardness in calcite by incorporation of amino acids. Nat Mater. 2016;15:903–10
37. Callister WD, Rethwisch DG. Materials science and engineering : an introduction (eighth edition). eighth edi. John Wiley & Sons Inc.; 2009
38. Yamaguchi T, Tsuruda Y, Furukawa T, Negishi L, Imura Y, Sakuda S, et al. Synthesis of CdSe Quantum Dots Using *Fusarium oxysporum*. Materials (Basel). 2016;9:855
39. Tamura H, Nagahama H, Tokura S. Preparation of chitin hydrogel under mild conditions. Cellulose. 2006;13:357–64
40. Pérez-Huerta A, Suzuki M, Cappelli C, Laiginhas F, Kintsu H. Atom Probe Tomography (APT) Characterization of Organics Occluded in Single Calcite Crystals: Implications for Biomineralization Studies. C — J Carbon Res. 2019;5:50

Figure legends

Figure 1. Analysis of the organic matrices in a calcite prism of *Pinctada fucata*. a, b, Scanning electron microscopy image of the prismatic layer. a, Surface structure. b, Longitudinal structure. c, Transmission electron microscopy image of the cross-section of a calcite prism. The arrow shows interference fringes of equal inclination (black lines), which are observed in a single crystal, and which are interrupted by small-angle grain boundaries. d, Schematic illustration describing how to extract the organic matrices from calcite prisms. e, Structural formula of chitin, which is comprised of *N*-acetyl-D-glucosamine. f, Sodium dodecyl sulfate-polyacrylamide gel electrophoresis of the acid-soluble organic matrices (lane 1) and acid-insoluble detergent-soluble organic matrices (lane 2). The box shows main proteins of the organic network. g, Schematic diagram of PfCN (upper) and PfCB (lower).

Figure 2. Synthesis of calcium carbonate crystals with chitin and chitinolytic enzymes. a, Schematic illustration describing the method of crystallization. b–d,

Scanning electron microscopy images of the synthesized calcium carbonate crystals in a chitin gel treated with chitinolytic enzymes at different concentrations or in chitin nanofiber solution. b, 0 mg/mL; c, 0.12 mg/mL; and d, 1.2 mg/mL chitinolytic enzymes; and e, chitin nanofiber solution. Dotted lines show the steps of crystals. The steps increased as chitin became thinner. Increasing steps is likely to make crystal shape round.

Figure 3. Analysis of the synthesized calcium carbonate crystals. a–d, Transmission electron microscopy images of a cross-section of synthesized calcium carbonate crystals in a chitin gel treated with chitinolytic enzymes at different concentrations or in chitin nanofiber solution. Low magnification (left) and high magnification (right). a, 0 mg/mL; b, 0.12 mg/mL; and c, 1.2 mg/mL chitinolytic enzymes; and d, chitin nanofiber solution. White arrows denote interference fringes of equal inclination and red arrows denote chitin fibers. White circles show that interference fringes of equal inclination are interrupted by small angle grain boundaries. e–h, Distribution of ions of the synthesized calcium carbonate crystals analyzed by atom probe tomography from a direction parallel to a longitudinal crystal. e, 0 mg/mL; f, 0.12 mg/mL; and g, 1.2 mg/mL chitinolytic enzymes; and h, chitin nanofiber solution. Clusters of some ions are observed. Red, Ca^{2+}; yellow, COH^{+}; and pink, COH^{2+}.

Figure 4. Change in mechanical properties following allosamidin injection. a, b, Microdiffraction maps of the prism calcites analyzed by electron backscatter diffraction. a, Non-injection. b, Allosamidin injection. Colors denote the orientation of calcite. Right graphs are line profiles from the origin to the end of arrows described in the maps. Red lines show an absolute value and blue lines show a relative value to the previous point. c,

d, Force-displacement curves measured by nanoindentation. c, Non-injection measured at eight points. d, Allosamidin injection measured at six points. A force was loaded up to 100 mN, followed by unloading. Blue denotes the spread of displacement. e, Hardness and reduced elastic modulus calculated from nanoindentation data.

Figure 1

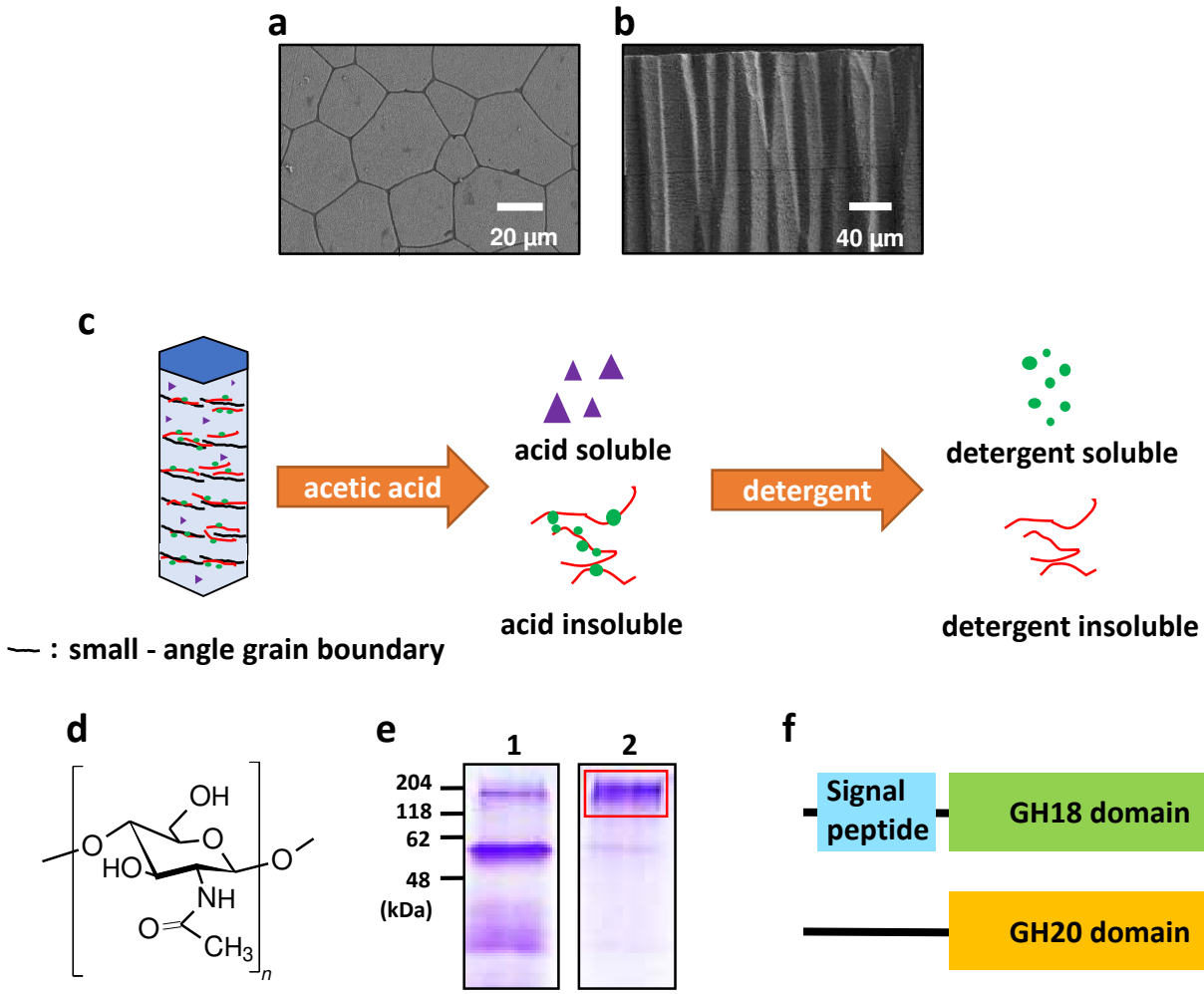
a
20 μm
b
40 μm
c
acetic acid
acid soluble
acid insoluble
detergent
detergent soluble
detergent insoluble
— : small - angle grain boundary
d
OH
O
HO
O
NH
O
CH3
n
e
1
2
204
118
62
48
(kDa)
f
Signal peptide
GH18 domain
GH20 domain

Figure 2

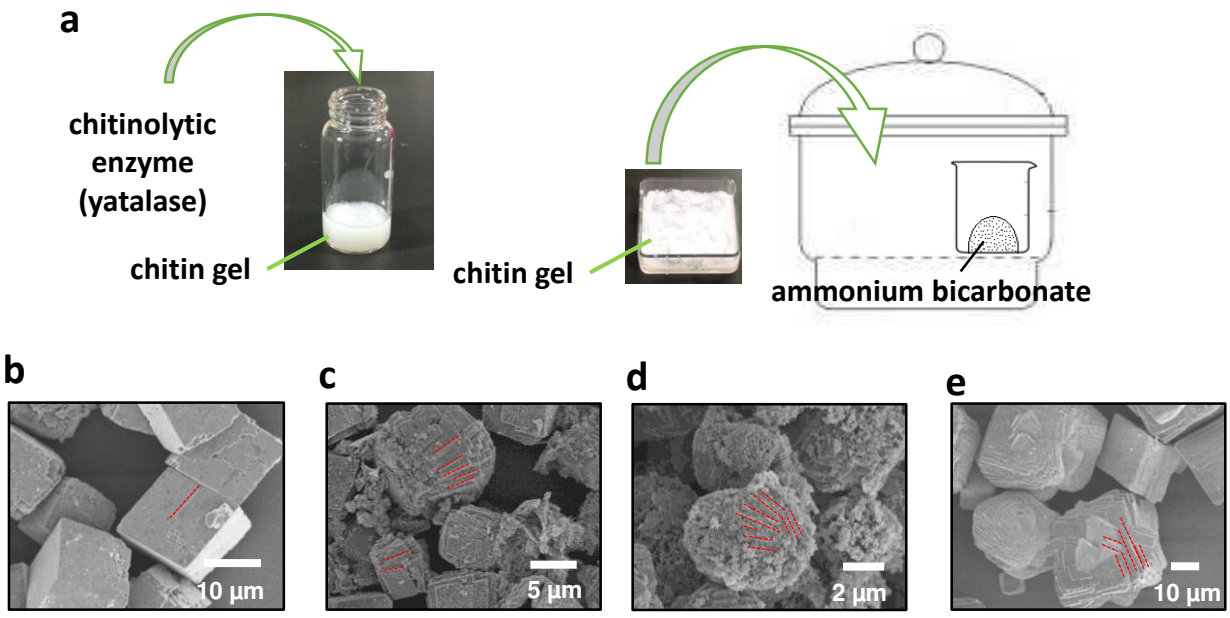
a
chitinolytic enzyme (yatalase)
chitin gel
chitin gel
ammonium bicarbonate
b
10 µm
c
5 µm
d
2 µm
e
10 µm

Figure 3

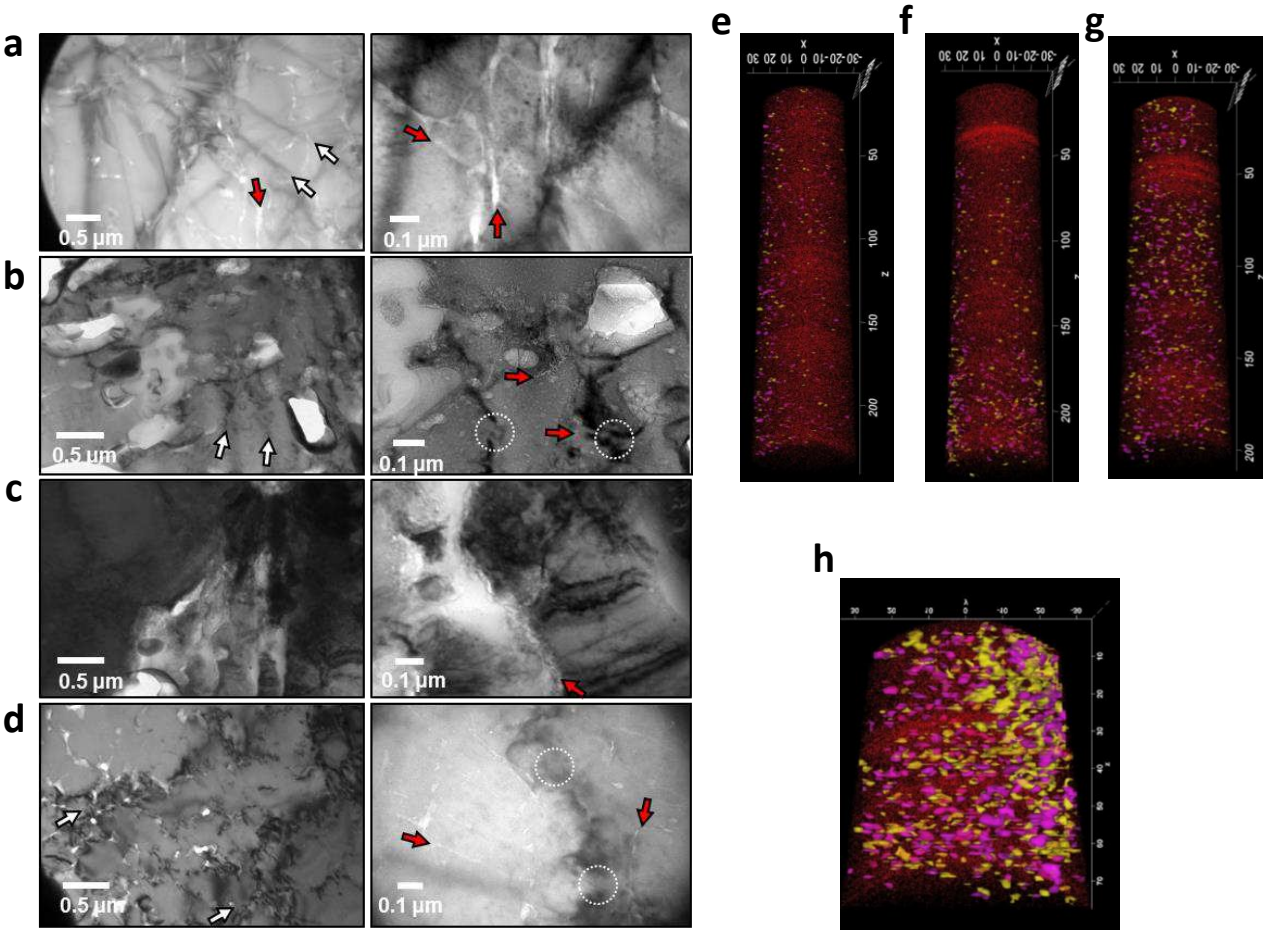

Figure 4

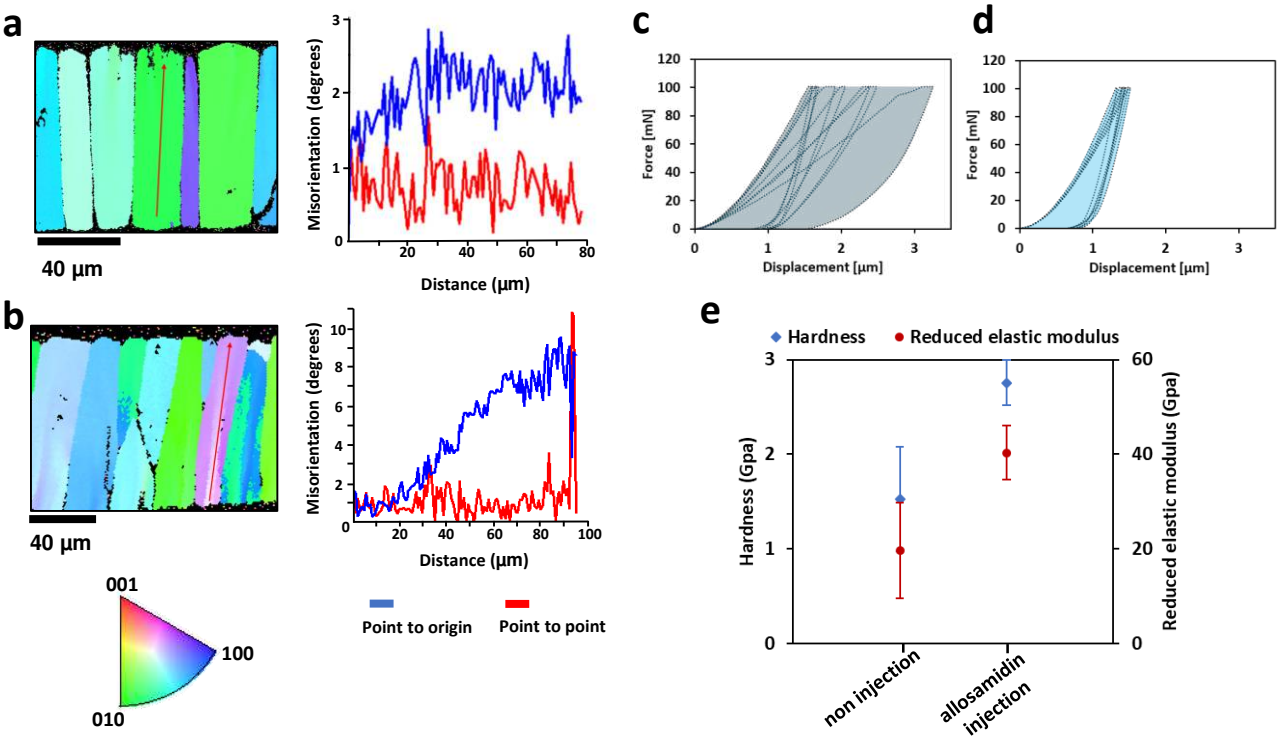
a
40 µm
Misorientation (degrees)
Distance (µm)
b
40 µm
001
100
010
Misorientation (degrees)
Distance (µm)
Point to origin
Point to point
c
Force [mN]
Displacement [µm]
d
Force [mN]
Displacement [µm]
e
Hardness
Reduced elastic modulus
Hardness (Gpa)
Reduced elastic modulus (Gpa)
non injection
allosamidin injection

Figure S1

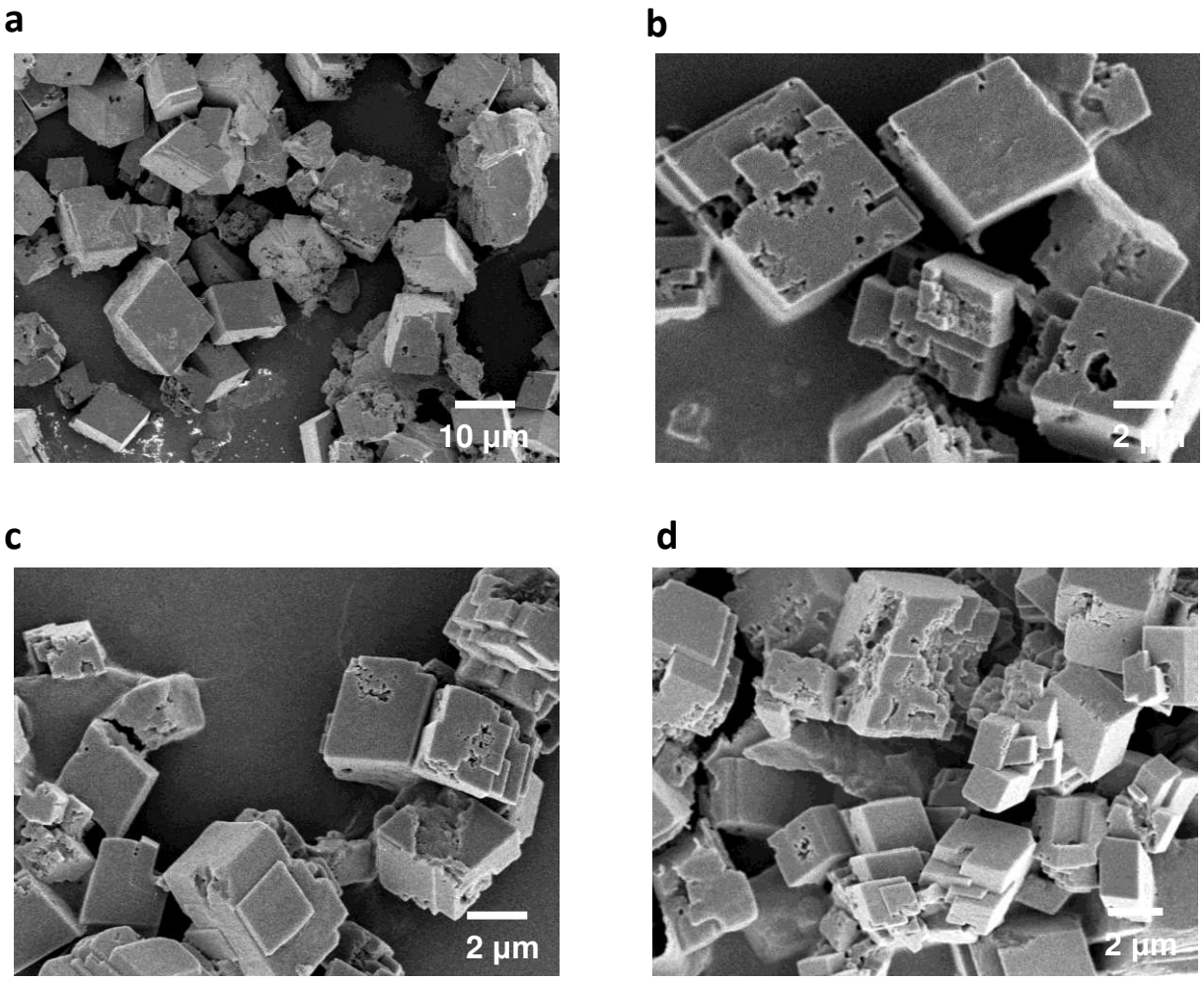

Supplementary Figure 1. Calcites synthesized in cellulose gel treated with cellulase at different concentrations.

a, 0 mg/mL; b, 0.012 mg/mL; c, 0.12 mg/mL; and d, 1.2 mg/mL cellulase. Rhombohedral shape, which is a typical shape of calcite, was observed at all conditions, indicating that cellulose had no effects on calcium carbonate crystallization.

Figure S2

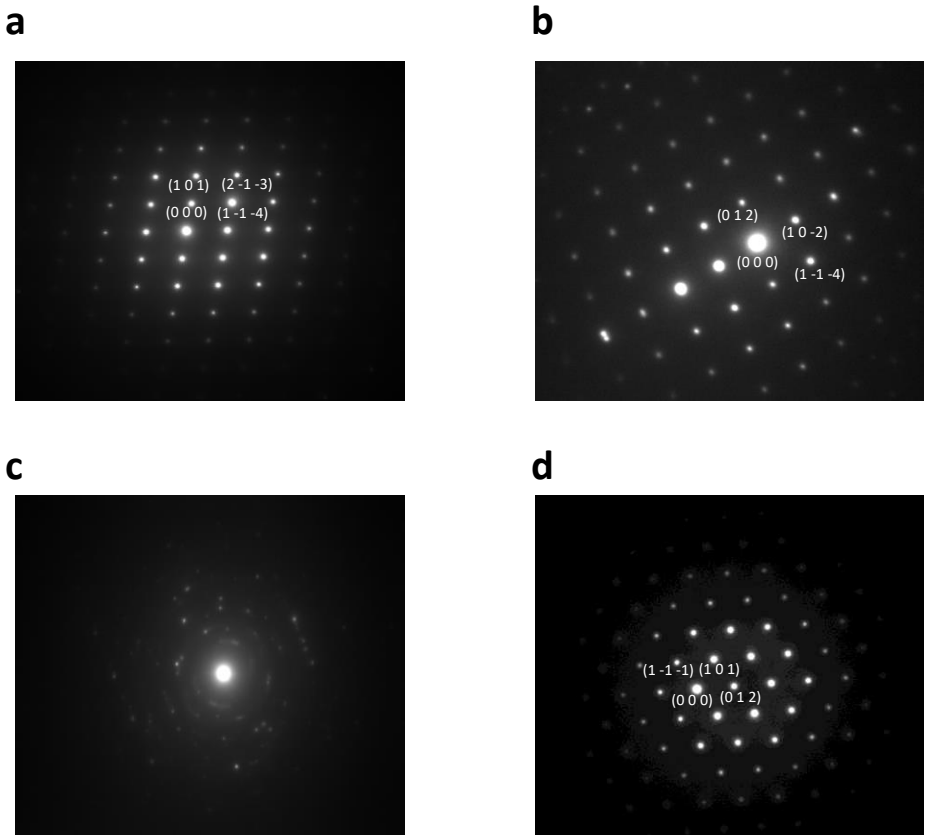

Supplementary Figure 2. Diffraction patterns of calcites synthesized in chitin gel treated with chitinolytic enzymes at different concentrations or in chitin nanofiber solution.

a, 0 mg/mL; b, 0.12 mg/mL; c, 1.2 mg/mL chitinolytic enzymes; and d, chitin nanofiber solution.

Figure S2

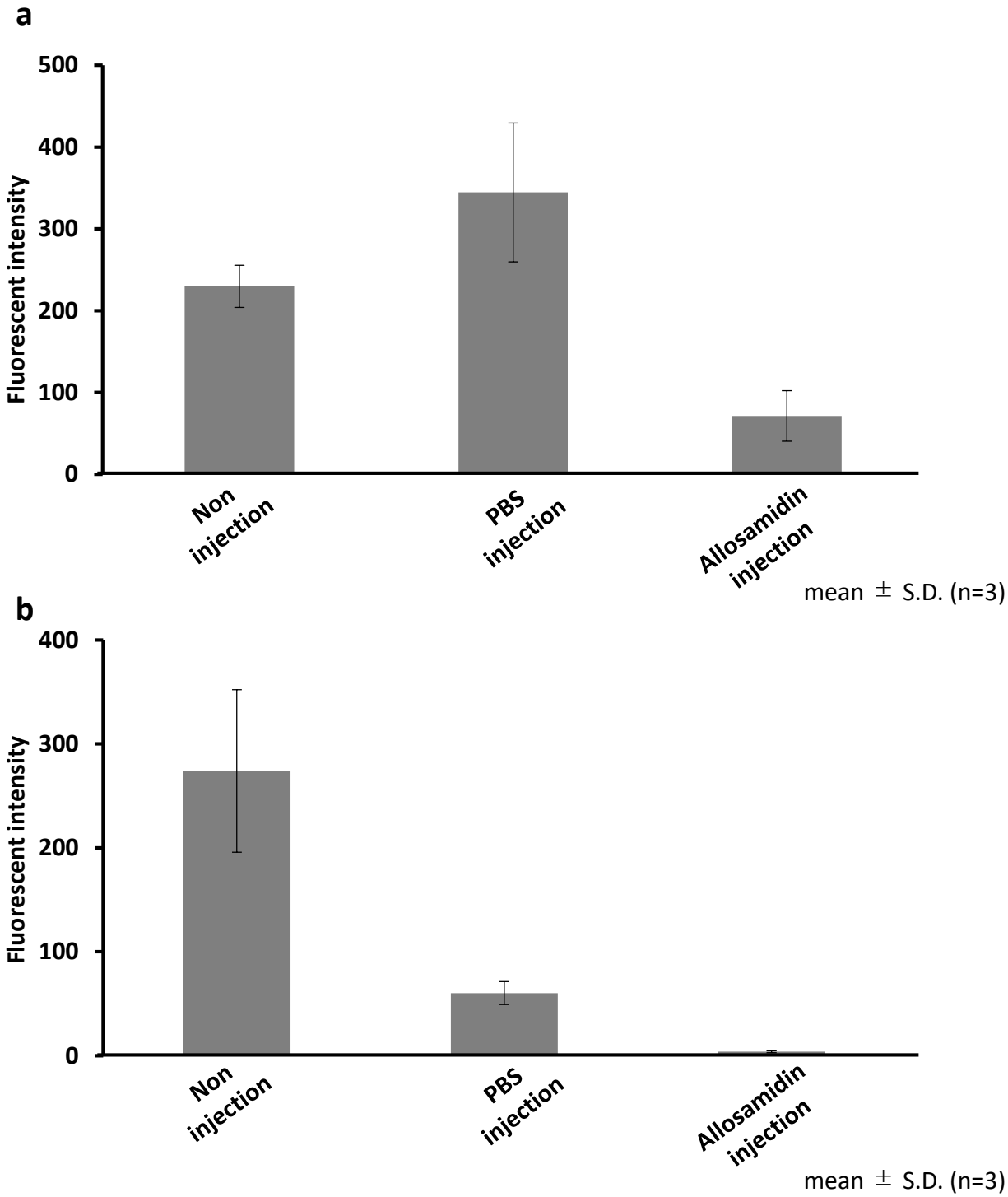

Supplementary Figure 3. Activity of chitinolytic enzymes from mantle tissue. Activity was measured (a) 4 days and (b) 32 days after the first injection of allosamidin. A concentration of total proteins of each solution extracted from the mantle tissue was aligned at 125 μg/mL using an absorption spectrophotometer. Fluorescence intensity of substances liberated from the substrate by chitinolytic enzymes was measured as the chitinolytic activity.

Figure S3

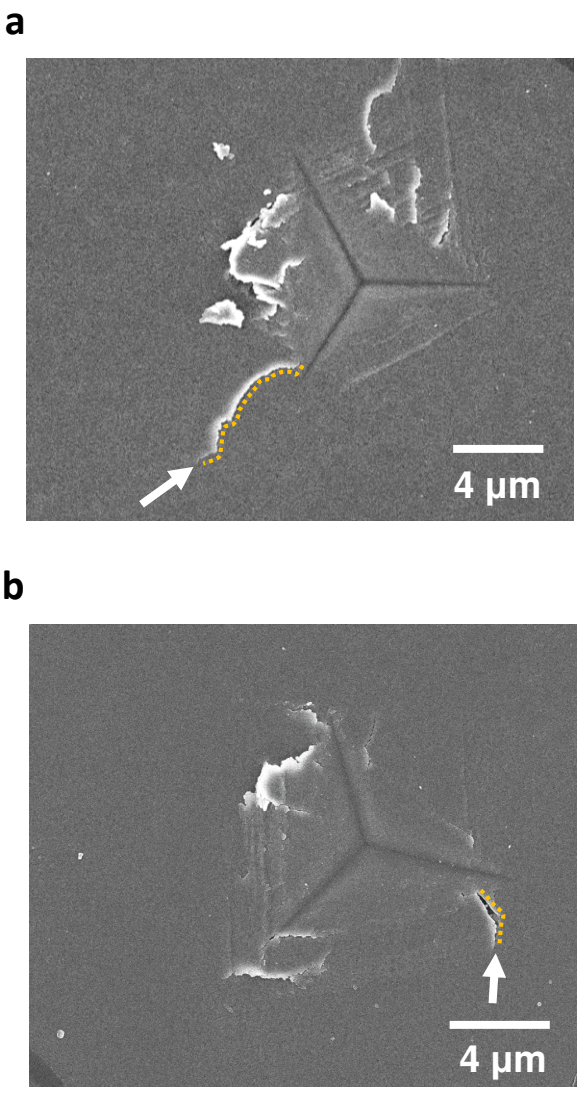

Supplementary Figure 4. Scanning electron microscopy images of the impression on the calcite prism after nanoindentation.
a, Non-injection. b, Allosamidin injection. Arrows denote a crack caused by nanoindentation. The crack penetration on (b) was inhibited when compared with (a) as described by arrows and dotted lines.

Figures

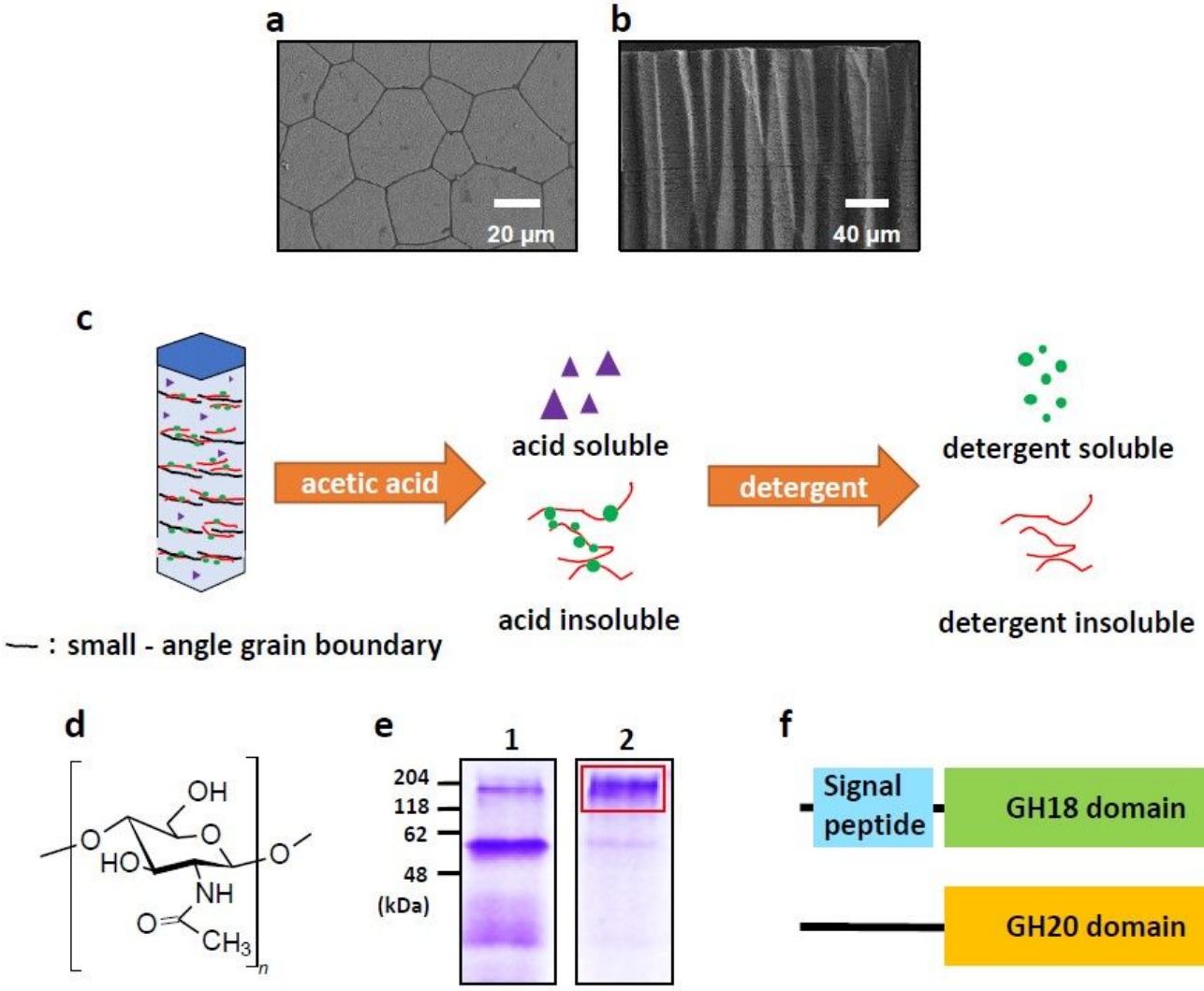

Figure 1

Analysis of the organic matrices in a calcite prism of Pinctada fucata. a, b, Scanning electron microscopy image of the prismatic layer. a, Surface structure. b, Longitudinal structure. c, Transmission electron microscopy image of the cross-section of a calcite prism. The arrow shows interference fringes of equal inclination (black lines), which are observed in a single crystal, and which are interrupted by small-angle grain boundaries. d, Schematic illustration describing how to extract the organic matrices from calcite prisms. e, Structural formula of chitin, which is comprised of N-acetyl-Dglucosamine. f, Sodium dodecyl sulfate-polyacrylamide gel electrophoresis of the acidsoluble organic matrices (lane 1) and acid-insoluble detergent-soluble organic matrices (lane 2). The box shows main proteins of the organic network. g, Schematic diagram of PfCN (upper) and PfCB (lower).

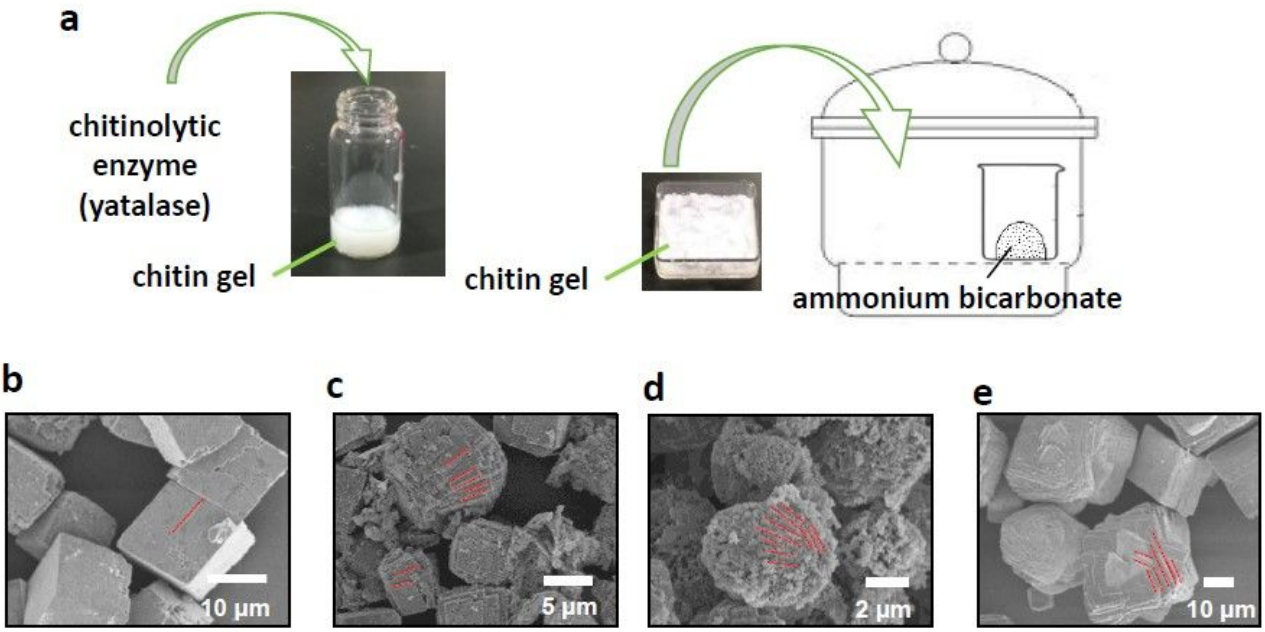

Figure 2

Synthesis of calcium carbonate crystals with chitin and chitinolytic enzymes. a, Schematic illustration describing the method of crystallization. b–d, 21 Scanning electron microscopy images of the synthesized calcium carbonate crystals in a chitin gel treated with chitinolytic enzymes at different concentrations or in chitin nanofiber solution. b, 0 mg/mL; c, 0.12 mg/mL; and d, 1.2 mg/mL chitinolytic enzymes; and e, chitin nanofiber solution. Dotted lines show the steps of crystals. The steps increased as chitin became thinner. Increasing steps is likely to make crystal shape round.

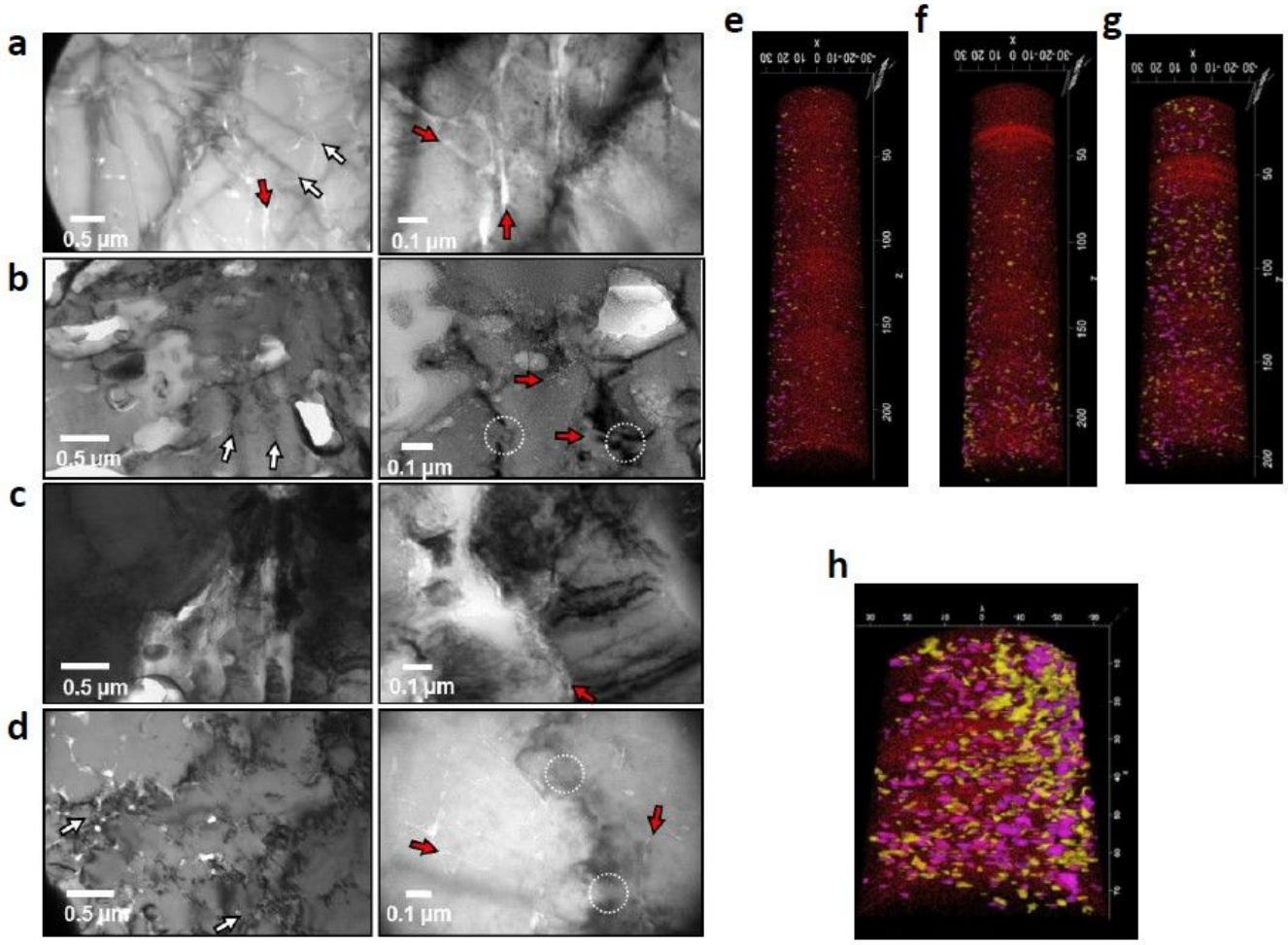

Figure 3

Analysis of the synthesized calcium carbonate crystals. a–d, Transmission electron microscopy images of a cross-section of synthesized calcium carbonate crystals in a chitin gel treated with chitinolytic enzymes at different concentrations or in chitin nanofiber solution. Low magnification (left) and high magnification (right). a, 0 mg/mL; b, 0.12 mg/mL; and c, 1.2 mg/mL chitinolytic enzymes; and d, chitin nanofiber solution. White arrows denote interference fringes of equal inclination and red arrows denote chitin fibers. White circles show that interference fringes of equal inclination are interrupted by small angle grain boundaries. e–h, Distribution of ions of the synthesized calcium carbonate crystals analyzed by atom probe tomography from a direction parallel to a longitudinal crystal. e, 0 mg/mL; f, 0.12 mg/mL; and g, 1.2 mg/mL chitinolytic enzymes; and h, chitin nanofiber solution. Clusters of some ions are observed. Red, Ca2+; yellow, COH+; and pink, COH2+.

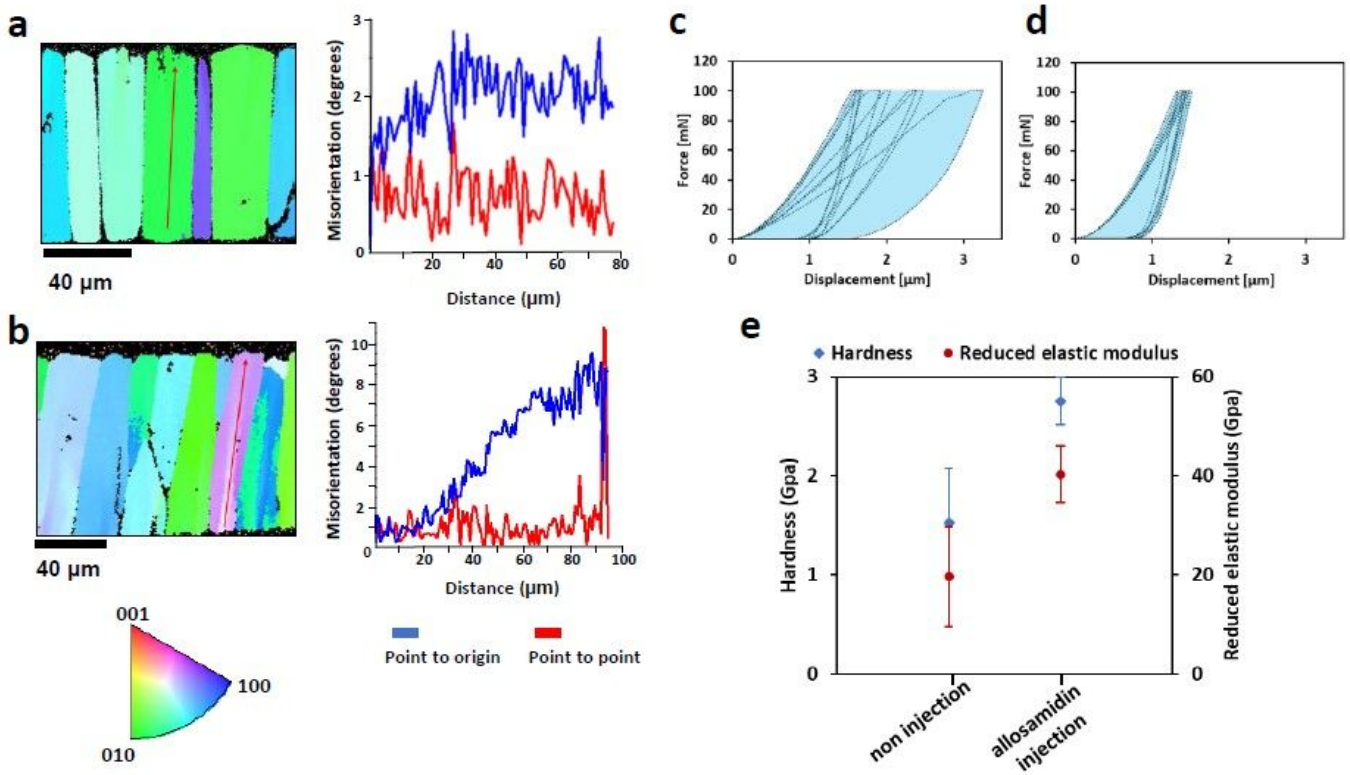

Figure 4

Change in mechanical properties following allosamidin injection. a, b, Microdiffraction maps of the prism calcites analyzed by electron backscatter diffraction. a, Non-injection. b, Allosamidin injection. Colors denote the orientation of calcite. Right graphs are line profiles from the origin to the end of arrows described in the maps. Red lines show an absolute value and blue lines show a relative value to the previous point. c, 22 d, Force-displacement curves measured by nanoindentation. c, Non-injection measured at eight points. d, Allosamidin injection measured at six points. A force was loaded up to 100 mN, followed by unloading. Blue denotes the spread of displacement. e, Hardness and reduced elastic modulus calculated from nanoindentation data.

Supplementary Files

This is a list of supplementary files associated with this preprint. Click to download.

- S1.jpg
- S2.jpg
- S3.jpg

- S4.jpg